Astron. Astrophys. 149, 135–143 (1985)

ASTRONOMY AND ASTROPHYSICS

A refined particle method for astrophysical problems

J. J. Monaghan[1,2] **and J. C. Lattanzio**[2]

[1] Max-Planck-Institut für Physik und Astrophysik, Karl-Schwarzschild-Strasse 1, D-8046 Garching bei München, Federal Republic of Germany
[2] Department of Mathematics, Monash University, Clayton, Victoria, 3168, Australia

Received April 10, 1984; accepted February 5, 1985

Summary. A version of the particle method SPH with greatly increased efficiency is described. The increase in efficiency is due to the use of a grid both for the calculation of gravitational forces and for the determination of nearest neighbours. Sufficient accuracy is achieved on coarse grids by the use of a short range correction for the gravitational force. Storage problems are thereby eliminated. Other improvements include the use of interpolation kernels based on *B*-splines, the use of particles with different masses and the use of a simple efficient artificial viscosity. A wide variety of tests confirm the overall accuracy.

Key words: hydrodynamics – numerical methods – particle methods – stars: formation of

1. Introduction

The purpose of this paper is to describe improvements to the current form of the particle method SPH (Gingold and Monaghan, 1977, 1982), which enable much larger numbers of particles to be used. The improvements results in the number of computations per time step being proportional to the number of particles. This improvement in speed is due primarily to the use of a grid based method for the calculation of the gravitational forces. A further substantial increase in efficiency is achieved by using the same grid to determine nearest neighbours through link lists.

The flexibility of the method has been improved by allowing the particle masses to be different. This enables complicated initial states to be set up with negligible fluctuation. An analysis of the equations of motion when the particles have different masses is given in Sect. 2. This analysis is particularly important because incorrect estimates of the errors in particle methods, and incorrect statements concerning the relationship between particle and finite difference methods, have appeared in the literature. Finite difference methods are just particle methods where the particles are fixed and have a mass which varies with time.

The interpolation kernels differ from those used by other authors (Gingold and Monaghan, 1977; Lucy, 1977; Wood, 1981). The kernels are discussed in Sect. 3.

The plan of the paper is to describe the improvements in sufficient detail to allow the reader to reconstruct the algorithms we use and to show, by a wide variety of tests, that the algorithms are efficient and accurate.

Send offprint requests to: J. J. Monaghan

2. The particle equations of motion

In this section we show that particle methods can be established in a form that allows the particles to have different masses. This leads to a number of advantages particularly the case of setting up initial states and the representation of regions with lower than average density. We base our analysis on the discussion by Monaghan (1982) which assumed the particle masses were all equal.

The analysis of numerical algorithms for partial differential equations can be based (Monaghan, 1982) on linear interpolants of the form

$$\langle f(\boldsymbol{r})\rangle := \int f(\boldsymbol{r}')W(\boldsymbol{r},\boldsymbol{r}',h)\,d\boldsymbol{r}', \tag{1}$$

where $W(\boldsymbol{r},\boldsymbol{r}',h)$ is an interpolating kernel $f(\boldsymbol{r}')$ is the function interpolated and the integration is over the solution domain. The parameter h is a measure of the resolution such that features on a length scale $\ll h$ are strongly smoothed by the interpolation. For the remainder of this paper we shall assume the kernel has the form $W(\boldsymbol{r}-\boldsymbol{r}',h)$ since this form is sufficiently general to include most interpolation methods and the analysis is greatly simplified. A further condition on W is that

$$\int W(\boldsymbol{u},h)\,d\boldsymbol{u}=1\,.$$

When the information (function values) is given on a *uniform* grid the kernels can be chosen so that (1) can be written in the form

$$\langle f(\boldsymbol{r})\rangle := \sum_j \frac{f_j}{n_j} W(\boldsymbol{r}-\boldsymbol{r}_j,h)\,, \tag{2}$$

where n_j is the number density of grid points at the point $\boldsymbol{r}_j$ and the notation $A_j \equiv A(\boldsymbol{r}_j)$ has been used. For a uniform grid n_j is a constant.

Derivatives can be estimated in the same way. For example

$$\left\langle \frac{\partial f}{\partial x}\right\rangle := \int \frac{\partial f}{\partial x'} W(\boldsymbol{r}-\boldsymbol{r}',h)\,d\boldsymbol{r}'\,. \tag{3}$$

To put (3) in a convenient form we integrate by parts assuming that $fW\to 0$ on the boundary. This assumption is satisfied for most problems since the kernel vanishes rapidly when $|\boldsymbol{r}-\boldsymbol{r}'|\to\infty$. Thus

$$\left\langle \frac{\partial f}{\partial x}\right\rangle = -\int f \frac{\partial}{\partial x'} W(\boldsymbol{r}-\boldsymbol{r}',h)\,d\boldsymbol{r}'$$

or

$$\left\langle \frac{\partial f}{\partial x}\right\rangle = \frac{\partial}{\partial x}\langle f\rangle\,. \tag{4}$$

The expression (4) for the derivative, in conjunction with (2), reproduces the usual finite difference formula on a uniform grid.

A convenient technique for generating numerical algorithms is to choose a kernel, multiply the equation of interest by the kernel, and then integrate over the solution domain (Monaghan, 1982). The resulting equations can then be transformed, possibly with some approximations, so that they use interpolated quantities.

For example, starting with the momentum equation for an inviscid fluid with body force $-\nabla\Phi$, we obtain

$$\left\langle \frac{dv}{dt} \right\rangle = -\left\langle \frac{1}{\varrho}\nabla P \right\rangle - \langle \nabla\Phi \rangle , \tag{5}$$

which can be approximated by

$$\frac{\partial \langle \boldsymbol{v} \rangle}{\partial t} + \langle \boldsymbol{v} \rangle \cdot \nabla \langle \boldsymbol{v} \rangle = -\nabla \langle P \rangle / \langle \varrho \rangle - \nabla \langle \Phi \rangle . \tag{6}$$

Other approximations for the nonlinear terms will lead to different algorithms. Bearing in mind the fact that the constraints on W are weak it is clear that a wide variety of finite difference algorithms can be generated in this way.

Suppose now that the data points $\boldsymbol{r}_1, \boldsymbol{r}_2, \ldots, \boldsymbol{r}_N$ are not on a uniform grid but have a number density that varies in space. The interpolation formula (1) can still be written in the form (2) but the approximation is poorer than for the uniform grid. The error depends on the smoothness of the kernel (assuming f is infinitely differentiable) and the degree of disorder of the points. Monaghan (1982) estimates that the variation of the error with N in three dimensions in $O(1/N)$.

The interpolation points can be fixed or they can be moved. In the latter case it is common to refer to interpolation points as particles. Accordingly, we assign to the interpolation point $\boldsymbol{r}_i$ a mass $\boldsymbol{m}_i$, a velocity $\boldsymbol{v}_i$ which is the velocity of the fluid at $\boldsymbol{r}_i$, and refer to it as particle i. The usual finite difference schemes on a fixed grid can be considered to be particle methods where the particles have zero velocity and a mass which varies with time.

The mass density $\varrho(\boldsymbol{r})$ can be estimated using (2) and replacing n_j by ϱ_j/m_j (this is the crucial step which introduces the particle masses) then

$$\langle \varrho(\boldsymbol{r}) \rangle = \sum_j m_j W(\boldsymbol{r}-\boldsymbol{r}_j, h) , \tag{7}$$

and total mass is conserved provided

$$\int \langle \varrho(\boldsymbol{r}) \rangle d\boldsymbol{r} = \sum_j m_j \tag{8}$$

is constant.

The particle form of the continuity equation has some interesting features. If the interpolation points move with a velocity $\boldsymbol{v}^*$ that need not be the fluid velocity, the continuity equation can be written

$$\frac{\delta}{\delta t}\langle \varrho \rangle + \nabla \cdot (\varrho \boldsymbol{v}) - \boldsymbol{v}^* \cdot \nabla \langle \varrho \rangle = 0 , \tag{9}$$

where $\delta/\delta t$ is the derivative following the motion of the points. Evaluating (9) at particle i we find

$$\sum_j \frac{\delta m_j}{\delta t} W_{ij} + \sum_j m_j \frac{\delta W_j}{\delta t} + \sum_j m_j \boldsymbol{v}_j \cdot \nabla_i W_{ij} - \Sigma m_j \boldsymbol{v}_i^* \cdot \nabla_i W_{ij} = 0 , \tag{10}$$

where $W_{ij} \equiv W(\boldsymbol{r}_i - \boldsymbol{r}_j)$. Since $\delta W_{ij}/\delta t = (\boldsymbol{v}_i^* - \boldsymbol{v}_j^*) \cdot \nabla_i W_{ij}$ (10) becomes

$$\sum_j \frac{\delta m_j}{\delta t} W_{ij} + \sum_j m_j (\boldsymbol{v}_j - \boldsymbol{v}_j^*) \cdot \nabla_i W_{ij} = 0 . \tag{11}$$

Equation (11) is a general continuity equation for particle methods. If the points move with the fluid $\boldsymbol{v}_j^* = \boldsymbol{v}_j$, then

$$\sum_j \frac{\delta m_j}{\delta t} W_{ij} = 0; \quad i = 1, 2, \ldots, N . \tag{12}$$

A natural solution of (12) is

$$\frac{\delta m_j}{\delta t} = 0; \quad j = 1, 2, \ldots, N , \tag{13}$$

so that, as expected, the particles should have fixed masses. In this case (8) is automatically satisfied.

If the particles are fixed $\boldsymbol{v}_j^* = 0$ and $\delta m_j/\delta t \equiv \partial m_j/\partial t$. For each particle we can allocate a cell of volume σ_j so that $m_j = \varrho_j \sigma_j$ and (11) becomes

$$\frac{\partial}{\partial t}\varrho_i + \nabla_i \cdot \sum_j \sigma_j \varrho_j \boldsymbol{v}_j W_{ij} = 0 , \tag{14}$$

which, with an appropriate W, is a finite difference form of the Eulerian continuity equation.

Various forms of the momentum equation have been discussed elsewhere (Gingold and Monaghan, 1982; Monaghan, 1982). The form we use in this paper is

$$\frac{d\boldsymbol{v}_i}{dt} = -\sum_j m_j \left(\frac{p_j}{\varrho_j^2} + \frac{p_i}{\varrho_i^2} \right) \nabla_i W_{ij} - \nabla_i \Phi_i , \tag{15}$$

which, if $m_j = m$, reduces to the equation used by Gingold and Monaghan. Provided W_{ij} is symmetric in i and j (the usual case) the pressure forces in (15) lead to exact conservation of linear and angular momentum.

It might be thought that a calculation with particles having different masses would lead to non-physical behaviour. There is no theoretical objection to using different masses, and the tests described in this paper confirm the theory. In a more stringent test (Monaghan and Pongracic, 1984) a shock diaphragm problem with an initial density ratio 4:1 was studied using both an equal mass configuration (and initial number density ratio 4:1) and a configuration with mass ratio 4:1 (and initial number density uniform). Both configurations gave nearly identical results.

In most astrophysical problems the gravitational force is obtained by solving Poisson's equation. In our notation

$$\nabla^2 \langle \Phi \rangle = 4\pi G \langle \varrho \rangle , \tag{16}$$

so that

$$\nabla_i^2 \langle \Phi \rangle_i = 4\pi G \sum_{j=1}^{N} m_j W_{ij} . \tag{17}$$

A solution of (17) which has been used in particle simulations is based on the fact that (17) is equivalent to spreading the mass of m_j according to the density W_{ij}. If W_{ij} is a function of $|\boldsymbol{r}_i - \boldsymbol{r}_j|$ it is easy to write down the potential and the force at $\boldsymbol{r}_i$ due to all other particles. Unfortunately, the number of arithmetic operations required to calculate this force for all particles is $\propto N^2$, which means that the computing time becomes prohibitively long for $N \gtrsim 10^3$. In Sect. 4, a grid based method for the solution of (16) will be described.

3. Interpolation kernels

The construction of interpolating kernels $W(u, h)$ is guided by the requirements of accuracy, smoothness and computational efficiency. Kernels can be compared by considering how they interpo-

late when the particles are on a regular grid with spacing h. We require $h\sim\Delta x$ since if $h\gg\Delta x$ the best resolution is not achieved. The kernel should interpolate with errors not exceeding $O(h^2)$ and at least the first derivative should be continuous so that (a) derivatives can be calculated and (b) slightly different particle positions have a negligible effect. Finally the kernel should be negligible if $|u|>\sigma h$ where $\sigma\sim 2$ otherwise too many particles contribute to local properties.

These considerations rule out the kernel $\propto\exp(-|u|/h)$ used by Wood (1981) since this kernel only gives accurate interpolation if $\sigma\gtrsim 4$ (this rule can be evaded for the density estimation by including a correction but it cannot be evaded for the estimation of derivatives). They also rule out kernels like $A(1-u^2/h^2)^4$ which are smooth but require $h\gg\Delta x$ in order to achieve approximate linear interpolation and good derivatives. The gaussian $\propto\exp(-u^2/h^2)$ has many desirable features: it is very smooth, and it interpolates linearly with high accuracy when $h=\Delta x$, but it requires $\sigma\gtrsim 3$. To improve the computational efficiency we look for kernels which have first or second derivative continuous, but which have compact support. Such kernels can be based on B-splines (M_n in Schoenberg's (1973) notation]. In one dimensional case the B-splines give exact linear interpolation on a uniform grid and their smoothness increases with n. Furthermore, they are non zero in a finite domain and this can make the calculations more efficient. Of particular importance are M_3 and M_4 which take the form

$$M_3(x)=\begin{cases}\frac{3}{4}-x^2; & 0\leqq|x|\leqq\frac{1}{2}\\ \frac{1}{2}(\frac{3}{2}-|x|)^2; & \frac{1}{2}\leqq|x|\leqq\frac{3}{2}\\ 0; & |x|\geqq\frac{3}{2}\end{cases}\tag{18}$$

which has a continuous first derivative and

$$M_4(x)=\begin{cases}\frac{2}{3}-x^2+\frac{1}{2}|x|^3; & 0\leqq|x|\leqq 1\\ (2-|x|)^3; & 1\leqq|x|\leqq 2\\ 0; & |x|\geqq 2\end{cases}\tag{19}$$

which has a continuous second derivative. Hockney and Eastwood (1981) recommend the use of $M_3(x)$ for calculating the grid density from the particles. For interpolation in 3 dimensions they use $M_3(x)M_3(y)M_3(z)$.

It will be seen later that for our gravitational field calculation it is necessary to have kernels which are spherically symmetric. In addition, the pressure forces will only conserve linear and angular momentum exactly if the kernels are spherically symmetric. A simple generalization of (18) and (19), and the one we adopt, is to replace them by

$$W_3(r,h)=\frac{1}{\pi h^3}\begin{cases}2(\frac{3}{4}-v^2); & 0\leqq v\leqq\frac{1}{2}\\ (\frac{3}{2}-v)^2; & \frac{1}{2}\leqq v\leqq\frac{3}{2}\\ 0; & v>\frac{3}{2},\end{cases}\tag{20}$$

$$W_4(r,h)=\frac{1}{\pi h^3}\begin{cases}\frac{3}{2}(\frac{2}{3}-v+\frac{1}{2}v^3): & 0\leqq v\leqq 1\\ \frac{1}{4}(2-v)^3; & 1\leqq v\leqq 2\\ 0; & v>2,\end{cases}\tag{21}$$

where $v=r/h$. The kernels are normalized so that

$$4\pi\int_0^\infty W_n(r,h)r^2dr=1\,.$$

These kernels do not achieve exact linear interpolation for all positions on a uniform three dimensional grid, but the error ($\pm 1\,\%$) varies in such a way that very accurate results are produced for an ensemble of particles.

The kernel W_3, is used for assigning a density to the grid points for the gravitational force calculation. The kernel W_4 is used for the density and pressure force calculation. W_4 could have been used for the density assignment, but it would require assignment to roughly double the number of vertices required for W_3.

Kernels which can interpolate with errors $O(h^3)$ can be obtained from the B-splines (Monaghan, 1984). When generalized to three dimensions a typical example is

$$W(r,h)=\frac{3}{4\pi h^3}\begin{cases}\frac{10}{3}-7v^2+4v^3; & 0\leqq v\leqq 1\\ (2-v)^2\left(\frac{5-4v}{3}\right); & 1\leqq v\leqq 2\\ 0; & v>2\,.\end{cases}\tag{22}$$

The choice of kernel has been partly dictated by the use we make of grids. The region occupied by the particles is divided into cubical cells of side $2h$. Only particles in neighbouring cells can contribute to each other's density and pressure forces. The particles are accessed through link lists.

The same set of cells is used for the finite difference calculation of the gravitational force. Therefore, when W_3 is used for the grid density assignment, h is replaced by $2h$.

4. The gravitational field calculation

The advantage of grid based methods is that they are quick. The disadvantage is that a very large grid may be needed to ensure that the resolution of a fragment is adequate. Storage then becomes a problem because a fragment may occupy $<10^{-2}$ of the total grid. One way to escape this difficulty is to use a relatively coarse grid, but make local corrections. This can be achieved by writing the solution of (16) in the form

$$\Phi(\boldsymbol{R})=-G\int\frac{\langle\varrho(\boldsymbol{r})\rangle}{|\boldsymbol{R}-\boldsymbol{r}|}d\boldsymbol{r}\,,\tag{23}$$

and replacing $\langle\varrho(\mathbf{r})\rangle$ by

$$\langle\varrho(r)\rangle^*+\langle\varrho(\boldsymbol{r})\rangle-\langle\varrho(\boldsymbol{r})\rangle^*\,,\tag{24}$$

where $\langle\varrho(\boldsymbol{r})\rangle^*$ is an interpolated density which uses an interpolating kernel $W^*(\boldsymbol{u},H)$ with a coarser resolution ($H>h$) than $W(u,h)$. Substituting (24) into (23) we find

$$\begin{aligned}&\Phi(\boldsymbol{R})=-G\int\frac{\langle\varrho(\boldsymbol{r})\rangle^*}{|\boldsymbol{R}-\boldsymbol{r}|}d\boldsymbol{r}-G\int\frac{(\langle\varrho(\boldsymbol{r})\rangle-\langle\varrho(\boldsymbol{r})\rangle)^*}{|\boldsymbol{R}-\boldsymbol{r}|}d\boldsymbol{r}\\ &\Phi(\boldsymbol{R})=\Phi^*(\boldsymbol{R})+\delta\Phi(\boldsymbol{R})\,.\end{aligned}\tag{25}$$

The first term Φ^* is the potential due to $\langle\varrho(\mathbf{r})\rangle^*$ which varies more smoothly than $\langle\varrho(\mathbf{r})\rangle$. It is this part of the potential which we calculate on the grid. The second term in (25) is a correction which only affects close neighbours. In most cases it is small, but it can greatly improve the self gravity calculated for a fragment.

The correction to the potential unit mass of particle i (from all other particles) is

$$-G\sum_{j=1}^{N}m_j\int\frac{[W(\boldsymbol{r}_j-\boldsymbol{r},h)-W^*(\boldsymbol{r}_j-\boldsymbol{r},H)]}{|\boldsymbol{r}_i-\boldsymbol{r}|}d\boldsymbol{r}\,,\tag{26}$$

and the correction to the grid force on particle i due to particle j is

$$\Delta F_{ij}=-\frac{Gm_j\boldsymbol{r}_{ij}}{r_{ij}^3}4\pi\int_0^{r_{ij}}[W(u,h)-W(u,H)]u^2du\,.\tag{27}$$

Since W and W^* are only non zero in a finite domain ΔF_{ij} is a short range force and it can be calculated at the same time as the pressure force. The cost of calculating the correction is therefore negligible.

The slowly varying part of the potential can be calculated by any of the well known Poisson solvers. We have found the multigrid method of Brandt (1977) to be very effective.

Once the potential is known on the grid the forces can be calculated by finite differences (we use central differences) and interpolated back to the particles. Hockney and Eastwood (1981) show that it is best to use the same interpolation kernels for the force interpolation as are used for the density assignment from the particles to the grid. The correction (27) to the grid force requires, in addition, that the interpolation kernels are spherically symmetric. These requirements are met by the kernel (20).

Because $W^*(u, H)$ is defined by (20) with h replaced by $2h$ (i.e. $H=2h$) it is non zero for $0 \leqq u \leqq 3h$. It is inconvenient to calculate the full short range correction because it would involve including particles in cells which are not nearest neighbours. We have therefore scaled W^* (by multiplying by 80/63) so that

$$4\pi\left(\tfrac{80}{63}\right) \int_0^{2h} W^*(u, H) u^2 du = 1 .$$

The result is that $\sim 75\%$ of the correction to the force is included. That this approximation is reasonable is shown by the results for the two-particle test in Sect. 6.1.

5. Numerical calculations

5.1. Scaling

We take the mass of the cloud M to be the unit of mass, a typical length scale R of the cloud to be the unit of length and the unit of time $\sqrt{R^3/GM}$. The scaled density D is then given by

$$D = \varrho (R^3/M) ,$$

the scaled pressure p is given by

$$P = D \frac{R_0 T}{\mu} \frac{R}{GM}$$

and the scaled potential ϕ by

$$\phi = \Phi\left(\frac{R}{GM}\right) .$$

5.2. Artificial viscosity

The constraints placed on the artificial viscosity are severe: it must be effective enough to allow shock phenomena to be simulated, but it must have negligible effect on angular momentum transport. We have found that for the configurations discussed in Sect. 6 the artificial viscosity described by Monaghan and Gingold (1983) or the very similar viscosity tested by Monaghan and Pongracic (1984) give satisfactory results. This latter viscosity requires replacing

$$\frac{p_i}{\varrho_i^2} + \frac{p_j}{\varrho_j^2}$$

in (15) by

$$\left(\frac{p_i}{\varrho_i^2} + \frac{p_j}{\varrho_j^2}\right)(1 - \alpha \mu_{ij}) , \tag{28}$$

where

$$\mu_{ij} = \begin{cases} \dfrac{\delta t \boldsymbol{v}_{ij} \cdot \boldsymbol{r}_{ij}}{r_{ij}^2 + \eta} ; & \text{if} \quad v_{ij} r_{ij} < 0 \\ 0 ; & \text{otherwise} \end{cases} \tag{29}$$

and δt is the time step. The viscosity only acts on approaching particles ($\boldsymbol{v}_{ij} \cdot \boldsymbol{r}_{ij} < 0$ is the particle equivalent of using the viscosity if $\nabla \cdot \mathbf{v} < 0$), and results in exact conservation of linear and angular momentum. For isothermal problems δt can be replaced by h/c where c is the speed of sound. For high Mach number collisions (Lattanzio et al., 1984) it is necessary to replace $1 - \alpha \mu_{ij}$ by $1 - \alpha \mu_{ij} + \beta \mu_{ij}^2$ which is equivalent to using both a regular bulk viscosity and a viscosity like the Von Neumann Richtmyer viscosity. In this case excellent results are obtained with $\alpha = \beta \cong 1$.

For some problems (e.g. that discussed in Sect. 9) it may be reasonable to use the viscosity only for the momentum component parallel to the rotation axis since planar shocks form above and below the equatorial plane. This also minimizes spurious angular momentum transport effects (Gingold and Monaghan, 1983). However, in general, one has to include viscosity in all three momentum components. Tests of angular momentum transport for this case are described by Monaghan and Lattanzio (1984).

5.3. Time differencing

We use the leap frog algorithm (Gingold and Monaghan, 1982) with a time step δt calculated by the following rules

(i) $S_i = \underset{i}{\text{Max}} (v_i^2 + c_i^2) ; \quad i = 1, 2, \ldots, N .$

(ii) $f = \underset{i}{\text{Max}} (\boldsymbol{F}_i^2)$ where $\boldsymbol{F}_i$ is the force on particle i.

(iii) $\delta t = 0.3 \, \text{Min}\left(\dfrac{h}{\sqrt{S}}, \sqrt{(h/f)}\right),$

where c_i is the speed of sound at particle i. For the two-particle tests with particle separation $= h$, the coefficient 0.3 in (iii) was replaced by 0.1 because the circumference of the orbit was only $\cong 3h$.

5.4. Variation of h

The value of h varies during the calculation according to the rule

$$h = \text{const} \bar{n}^{-1/3} ,$$

where $\bar{n}$ is the average number density defined by

$$\bar{n} = \frac{1}{N} \sum_j \varrho_j / m_j .$$

6. Tests of the gravitational force calculation

The multigrid algorithm was tested using the density $\sin \pi x \sin \pi y \sin \pi z$ in the domain $0 \leqq x, y, z \leqq 1$ for which the exact potential is known. This static test is useful for determining the optimum parameters for the multigrid method. These parameters were chosen so that the gravitational force had an error $< 0.1\%$ on a $20 \times 20 \times 20$ grid. In the following we describe dynamic tests.

6.1. Two-particle motion

A particularly stringent, but easily implemented dynamic test is to follow the motion of a binary. This tests all aspects of the potential

Table 1. J_z variation for binary orbits in the $x-y$ plane with separation 10h, 6h, 2h and h. The cell size is 2h

Time step	10 h	6 h	2 h	h
10	0.2502	0.1936	0.1130	0.06286
20	0.2502	0.1932	0.1080	0.06298
30	0.2504	0.1930	0.1073	0.06339
40	0.2499	0.1930	0.1102	0.06220
50	0.2497	0.1930	0.1082	0.06308
60	0.2497	0.1939	0.1037	0.06295
70	0.2498	0.1925	0.1047	0.06275
80	0.2501	0.1937	0.1049	0.06280
90	0.2503	0.1934	0.1066	0.06374
100	0.2502	0.1939	0.1130	0.06253
Max % variation from the mean J_z	0.16	0.40	4.0	1.1

calculation: the density assignment, the boundary conditions and the calculation and interpolation of the forces. In addition, because two particles, when they are close enough, produce a sharply varying potential, the test places severe demands on the potential solver. Furthermore, the test indicates how well the calculated gravitational force leads to angular momentum conservation. In the Eulerian picture the two-particle configuration represents a concentrated flow of matter and angular momentum through the mesh. The test therefore may also be viewed as a test of angular momentum transport.

In the calculations to be described two particles, each with mass 0.5, were started with a velocity which should produce a circular orbit in the $x-y$ plane. The grid occupied the domain $-2.0 \leqq x, y, z \leqq 2.0$ and the surface potential was calculated using all multipole moments up to the $6th$. The value of h was 0.1 making the cell width 0.2. In Table 1 we show the variation of the z component of the angular momentum for various particle separations. The widest binary examined had an initial separation of 5 cell widths. The closest binary had a separation of 0.5 cell widths.

For all separations the nett gain or loss of angular momentum is negligible. The variation in angular momentum during the orbital motion is slight for initial separations >2 cell widths. It is larger for motion taking place entirely within a cell, but the short range correction keeps the variation $<4\%$ for all motion within the cell.

The conservation of J_z shows that the grid force + correction maintains a very good approximation to a central force. For binaries with separation $>2h$ the principal error term is due to a small dipole component in the potential. An alternative way of looking at this error is that the potential between two particles, which should be

$$-\frac{Gm_1m_2}{|r_1-r_2|}, \tag{30}$$

is approximated by

$$-\frac{Gm_1m_2}{|r_1-r_2-\varepsilon|}, \tag{31}$$

where ε is a constant vector. For example, the orbit shown in the left frame of Fig. 1 should be a circle with centre origin. The effect of the potential (31) is to produce circular orbits for each particle with one orbit centred on $\varepsilon/2$ and the other centred on $-\varepsilon/2$.

The dipole perturbation produces no nett change to J_z when J_z is averaged over an orbit. The effect of the perturbation decreases with increasing binary separation so that the errors in the orbit of a binary with separation 5 cell widths are $\lesssim$ half those with separation 3 cell widths.

For two particles with separation less than a cell width, the deviation from the inverse square force law becomes more pronounced. The major effect is due to the fact that the particle's mass appears to be smoothed out and, even if the correction we used was perfect, the particle would appear smoothed out on a scale $\sim h$. Superimposed on this effect are errors arising from the use of a grid e.g. the dipole term described above. Because the force is no longer inverse square the orbit does not return to its original position as shown in the right frame of Fig. 1. If the short range correction is not included the particles leave the cell on an orbit with maximum range $\gtrsim$ two cell widths. The small variation of J_z for this orbit shows that effects due to the structure of the grid are not important. This is all the more remarkable when it is realized that the boundary of the right frame of Fig. 1 is that of an entire cell.

Typical limits on the other components of J are, for a separation of 3 cell widths, $|J_x| < 6\,10^{-5}$. The excursion out of the $x-y$ plane is typically <0.0005. The linear momentum varies about zero with an amplitude of $<4\,10^{-4}$.

The simulation of a gas cloud presents less stringent problems of angular momentum transport than are posed by the two-body problem and the conservation and transport of angular momentum in rotating gas clouds should be better. Results in the

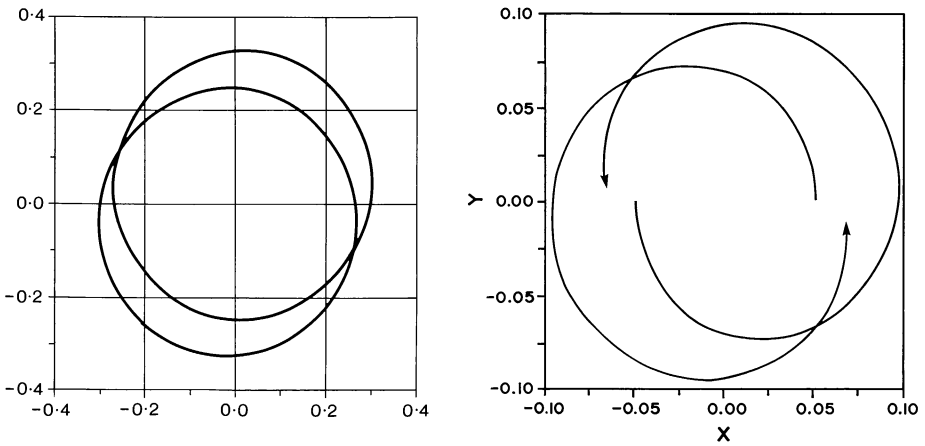

Fig. 1. Orbits of a binary (two particles) with mass ratio 1:1. The cell width is 0.2. Left frame: initial separation is $6h \equiv 3$ cells. The exact orbit is a circle with centre the origin. Right frame: initial separation is $h \equiv 0.5$ cell widths. The orbits of both particles are shown. In the absence of the gravitational correction the orbits leave the cell

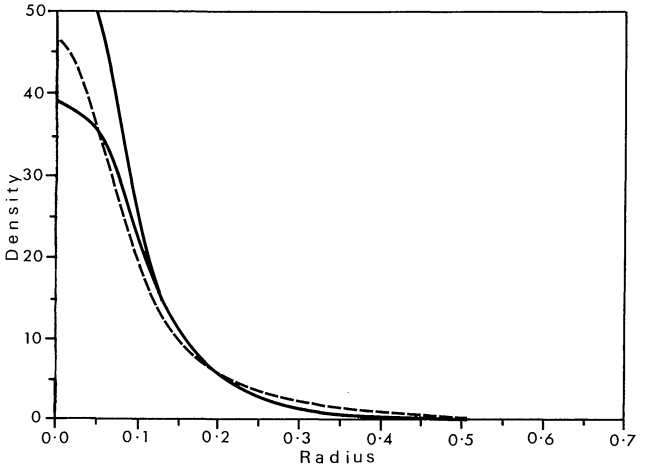

Fig. 2. The density profile for the collapse of a pressureless spherically symmetric cloud with initial $D=(21/16\pi)(1-r^4)$. The SPH results using 3544 particles $t=0.807$ when $h=0.041$ shown: —. Exact density at $t=0.807$ shown: – – – – (upper curve) and at $t=0.800$ shown: – – – – (lower curve)

following sections confirm these expectations. For example, the axisymmetric collapse of a cloud rotating about the z axis results in $|\Delta J_z/J_z|<10^{-4}$.

6.2. Spherical collapse – zero pressure

Several tests of spherical collapse were examined using both equal and different mass particles. The test we describe here had an initial density

$$D=\frac{21}{16\pi}(1-r^4);\quad 0\leqq r\leqq 1,$$

and the particles were initially set on a uniform cartesian grid with cell width 0.1 and initial $h=0.1$. The particle ar $\mathbf{r}_i$ was given a mass $m_i=D_i(0.1)^3$, where D_i is the density at $\mathbf{r}_i$. Only those particles (3544 in all) within the sphere of radius $r=1.0$ were included.

For this model the shells with radii (0.25, 0.5, 0.9) reach the centre at times (0.84, 0.85, 0.99).

In Fig. 2 we compare the SPH results at $t=0.807$ with the exact results at $t=0.807$and at $t=0.800$. The SPH results agree best with the exact results at the slightly earlier time. When compared with a standard Lagrangian finite difference scheme, using spherical shells which initially have equal separation, the SPH results are better than those from a 20 shell finite difference calculation and nearly comparable to those from a 50 shell calculation. These finite difference calculations give a better description of the envelope because the SPH method with a single h biased towards the high density regions gives a poor representation of the density in the very low density regions. It should, however, be kept in mind that a 20 shell finite difference calculation is roughly equivalent to $(40)^3=64{,}000$ cells in three dimensions so the SPH calculation with 3544 particles is remarkably successful.

7. Spherical collapse – with non-zero pressure

The spherically symmetric isothermal collapse of a gas cloud provides a test of the pressure force calculation. For the results to be described

$$D=\frac{12}{16\pi}\left(1-\frac{4\pi}{3}D_{\text{ext}}\right)(1-r^4)+D_{\text{ext}}$$

with $D_{\text{ext}}=0.1$. The equation of state was $p=0.2D$. We used 3544 different mass particles on an initially regular grid as described in Sect. 6.2. The outer boundary condition was an external pressure $p_{\text{ext}}=0.2D_{\text{ext}}$. The initial h was equal to 0.1.

In the left frame of Fig. 3 we show the density profile as a function of radius, and compare it to a 50 shell finite difference calculation. As was the case for the pressureless collapse the SPH profile is closer to the finite difference profile at a slightly earlier time. For this reason the SPH profile is shown for the time 0.82 while the finite different profile is at $t=0.78$. The finite difference profile at $t=0.82$ has a central density of 3.5, but is otherwise similar to the profile shown.

In the right frame of Fig. 3 we show the density profile at a later time when the similarity solution $\varrho\propto 1/r^2$ should apply except within $\sim h$ of the centre. It can be seen that the agreement with the similarity solution is very good.

These results indicate that the pressure forces are being calculated with satisfactory accuracy.

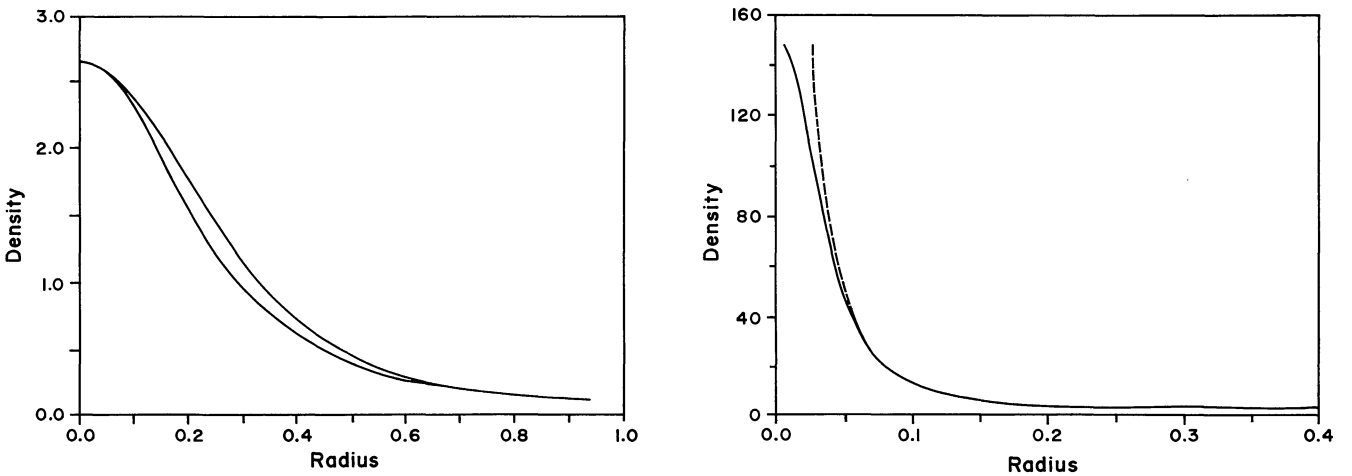

Fig. 3. Spherical collapse of a cloud with scaled equation of state $p=0.2D$. Left frame: upper curve 50 shell finite difference calculation at $t=0.78$. Lower curve SPH calculation (3544 particles) at $t=0.82$. Right frame: SPH results at $t=1.09$, when $h=0.033$, shown: —. The similarity solution shown: – – – –

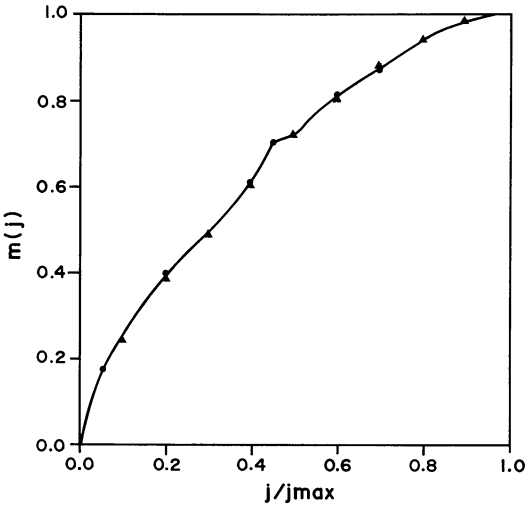

Fig. 4. The invariant $m(j)$ at $t=0$ shown: ● and at $t=1.006$ shown: ▲

8. The collapse of a rotating axisymmetric isothermal cloud

Since there are no exact solutions for this problem we regard it as a test of angular momentum transport and conservation.

If there is no spurious transport of angular momentum each particle retains its initial specific angular momentum. Accordingly $m(j)$, the mass with specific angular momentum $\leqq j$ will be invariant. In Fig. 4 we show $m(j)$ as a function of j for the collapse of an initial model with

$$D=\frac{3}{\pi}(1-D_0)(1-r)+D_0, \quad 0\leqq r\leqq 1,$$

where D_0 is the external density (taken as 0.2). The scaled equation of state was $p=0.1D$ and the initial angular velocity (about the z axis) was 0.70. The simulation used 3544 particles with initial $h=0.1$ and α, the viscosity parameter, was 7.0.

It is clear from Fig. 4 that the transport of angular momentum is very good. A more detailed analysis of the data shows that for 80% of the mass the deviation of $m(j)$ from the initial value is always $<0.5\%$. The deviation in the outer layers can be as large as one percent. These results together with those for the two body problem confirm that the pressure, viscous and gravitational forces lead to negligible errors in the transport of angular momentum.

The total z component of angular momentum deviated by $<5\,10^{-5}$ of its original value. The other components, initially zero, remained $<2\,10^{-6}$. The three components of linear momentum remained $<10^{-4}$.

In Fig. 5 we show two projections of the particles. The beautiful symmetry of these projections shows that the gravitational forces are accurately maintaining the equatorial reflection symmetry. It also confirms our suggestion that the particles always remain highly ordered. The outer layers are not axisymmetric because of the way we select particles from a cartesian grid. The particles in these layers have a negligible influence on the dynamics because their mass is very low.

9. Binary fragmentation

As a final test of the behaviour of the algorithm we simulated the collapse and fragmentation of the perturbed isothermal cloud considered by Boss and Bodenheimer (1979) and Gingold and Monaghan (1981) (referred to here as GM).

Because we use a particle method which is a refinement of that used in GM we expect similar results when the number of particles and the resolution are similar. The major differences between the simulation we describe, and that in GM, is that we use particles of different mass and the gravitational force is calculated using finite differences. The simulation therefore tests the extent to which the calculation is sensitive to these features.

The details of the initial cloud are given in GM. In terms of the scaled variables the density D is given by

$$D=\frac{3}{4\pi}\left(1+\frac{1}{2}\cos 2\phi\right),$$

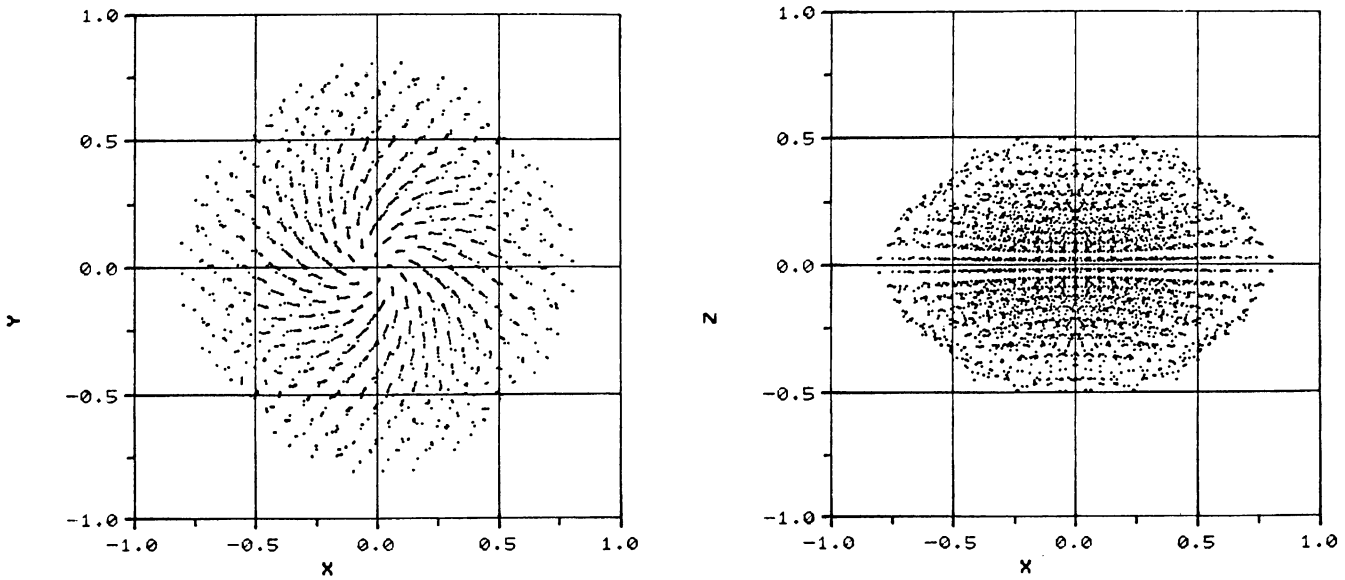

Fig. 5. Particle positions for the collapse of a rotating isothermal cloud. Left frame: positions projected onto the $x-y$ plane. Right frame: positions projected onto the $z-x$ plane

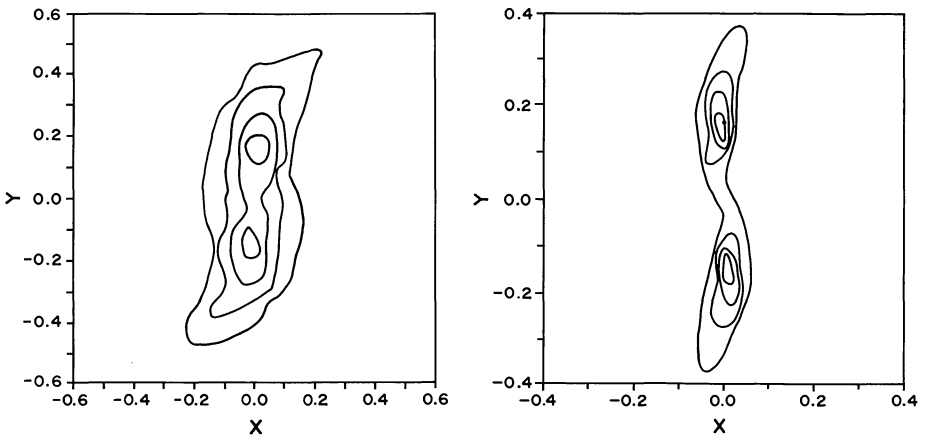

Fig. 6. Density contours for the collapse considered by Boss and Bodenheimer. The unit of length is $3.2\,10^{16}$ cms. Left frame: contours for a simulation using 3544 particles at $t=1.44$ ($2.3\,10^4$ yr) when $h=0.051$. The contours are for the following fractions of the maximum density 0.93, 0.75, 0.50, 0.25, 0.125. Right frame: SPH simulation using 7153 particles but rejecting those with density <0.05 maximum density. $t=1.51$ ($2.4\,10^4$ yr) when $h=0.032$. Note the scale change

which represents a perturbed uniform cloud. We define $D=3/(4\pi)$ on the rotation (z) axis. The equation of state is $p=0.1D$. The outer boundary was allowed to be a free surface. This boundary condition differs from the constant volume condition used by GM, but is is not expected to have a serious influence on the evolution.

Because the grid we use has a maximum size ($29\times29\times29$), and it is required to cover the entire set of particles, there is a minimum value of h that can be used. For the first simulation described below this minimum h was reached after ~1.5 free fall times (t_{ff}) and thereafter the h was up to twice that used in GM. To escape this difficulty we eliminated those particles with a density less than some specified fraction of the maximum density. This technique was used in the second simulation.

The first simulation used 3544 particles with initial $h=0.1$. The particles were initially on a uniform cartesian grid with cell width $l=0.1$. The mass of particle i at the position with density D_i was set at $D_i l^3$. Artificial viscosity was used only for the momentum parallel to the rotation axis. The simulation was run until $t=3.3\,10^4$ yr ($\sim 2t_{ff}$) when the maximum density had increased by 153. This density was lower than that in GM by a factor ~3. The reason for the lower density is that h is being determined by the maximum grid size and at this time it is twice the h used in GM. In other aspects the growing fragments followed the evolution described in GM. In the left frame of Fig. 6 we show the density contours for $t=2.3\,10^4$ yr. They are similar to, but less compact than, those found by GM. The fragments eventually coalesce. The initial J_z was 0.3030 and the final J_z was 0.3036. The other components of angular momentum remained, in magnitude, $\sim10^{-5}$.

A second simulation was run using 7153 particles with initial $h=0.08$. Particles with density $\leqq0.05$ of the maximum density were rejected until the number of particles were reduced to 3068. In the right frame of Fig. 6 we show the density contours at $t=2.5\,10^4$ yr. The density contours have now altered, as might be expected since the h for this simulation at this time is half the h for the previous simulation. The overall evolution of the cloud is similar to that found by GM. The fragments in our simulation reach a maximum density within 20% of that found by GM and the density varied in a similar fashion. The fragments move on a similar orbit to that found for the 3544 particle simulation and they eventually coalesce.

These results confirm that our calculation of the gravitational field reproduces the SPH results found using a gravitational field calculated by direct summation over the particles. The use of different mass particles does not introduce spurious results.

Full details of this and other collapse sequences will be published elsewhere.

10. Discussion and conclusions

The static tests referred to in Sect. 6 show that, for densities which vary on a scale of several cells, the gravitational force is obtained with errors $<0.1\%$. The two-particle tests of Sect. 6 show that the calculated forces give excellent conservation of linear and angular momentum even for orbits within a computational cell. The magnitude of the force has a larger error than is the case for the slowly varying density because each of the two particles forming the binary assigns a density to the nearest vertices of the grid. The density therefore varies rapidly on the scale of one cell. Despite this the force is in error by only $\sim5\%$ when the particles are separated by 3 cells. The error decreases rapidly with increasing separation.

It is more difficult to make error estimates from the tests based on the spherically symmetric collapse of a cloud because the finite differencing in time has the effect of delaying the collapse. If account is taken of the delay, which is normally a few percent of the actual time, the agreement with high accuracy finite difference calculations is very good.

The collapse of rotating clouds provides evidence of the conservation and transport of angular momentum within the cloud. The detailed results described in Sects. 8 and 9 show that the algorithm conserves and transports angular momentum very accurately and that no spurious effects are introduced by the use of particles with different masses.

The refined version of SPH which we have described is capable, when programmed carefully, of handling $\sim10^4$ particles on a Vax 11/780. The main points to keep in mind when programming for components like the Vax 11 are

(i) access particles through link lists or their equivalent,
(ii) relabel particles to reduce page faults, and
(iii) calculate kernels by interpolation from an array.

Acknowledgements. The hospitality of the Max-Planck-Institute for Astrophysics, Garching where this paper was written is gratefully acknowledged.

This work was supported by ARGS grant B8215094I.

References

Boss, A.P., Bodenheimer, P.: 1979, *Astrophys. J.* **234**, 289
Brandt, A.: 1977, *Math. Comp.* **31**, 333
Gingold, R.A., Monaghan, J.J.: 1977, *Monthly Notices Roy. Astron. Soc.* **181**, 375
Gingold, R.A., Monaghan, J.J.: 1981, *Monthly Notices Roy. Astron. Soc.* **197**, 461

Gingold, R.A., Monaghan, J.J.: 1982, *J. Comp. Phys.* **46**, 429
Gingold, R.A., Monaghan, J.J.: 1983, *Monthly Notices Roy. Astron. Soc.* **204**, 715
Hockney, R.W., Eastwood, J.W.: 1981, Computer simulation using particles, McGraw-Hill, New York
Lattanzio, J.C., Monaghan, J.J., Schwarz, M.P., Pongracic, H.: 1984 (preprint), Controlling Penetration
Lucy, L.B.: 1977, *Astron. J.* **83**, 1013
Beale, J.T., Majda, A.: 1982, *Math. Comp.* **39**, 1
Monaghan, J.J.: 1982, *Soc. In. App. Math. J. Sci. Stat. Comp.* **3**, 422
Monaghan, J.J.: 1984, Extrapolating *B*-splines for Interpolation, *J. Comp. Phys.* (in press)
Monaghan, J.J., Lattanzio, J.C.: 1984 (preprint), Further Studies of a Fragmentation Problem
Monaghan, J.J., Pongracic, H.: 1984, Artificial Viscosity for Particle Methods, *IMACS J. Num. Math.* (vol. and page not yet known)
Niederreiter, H.: 1978, *Bull. Amer. Math. Soc.* **84**, 957
Schoenberg, I.J.: 1973, Cardinal Spline Interpolation, *Soc. Ind. App. Math.*, Philadelphia, USA
Wood, D.: 1981, *Mounthly Notices Roy. Astron. Soc.* **194**, 201